

**PHOTOCATALYTIC DEGRADATION OF PHENOL IN
FLUIDIZED BED REACTOR USING TiO₂-P25/ACTIVATED
CARBON PREPARED BY MODIFIED SOL-GEL METHOD**

by

LAM SZE MUN

**Thesis submitted in fulfillment of the
requirements for the degree
of Master of Science**

MAY 2010

ACKNOWLEDGEMENTS

I am deeply grateful and sincerely thank my principal Supervisor, Prof. Abdul Rahman Bin Mohamed for his professional guidance, kind support, encouragement and caring throughout my study. I am also especially grateful to his valuable knowledge inputs and never being tired of reading my work.

I sincerely thank all the respective lectures, staffs and technicians of School of Chemical Engineering for their help given in either directly or indirectly. My special thanks go to Prof. Abdul Latif Ahmad, Assoc. Prof. Bassim H. Hameed, Dr. Zainal Ahmad, Pn. Aniza, En. Roqib, En. Mohd. Faiza and Pn. Latifah Latif for their support and assistance throughout my study. Thanks also go to the technicians of School of Material and Mineral Resources Engineering, School of Biological Science and School of Chemical Science for their help with sample analyses. I also express my sincere gratitude to my friends Sin Jin Chung, Nor Fauziah, Liu Wei Wen and Sivakumar for their advice, support and friendship throughout my study.

I gratefully acknowledge Universiti Sains Malaysia (USM) Fellowship, Ministry of Science, Technology and Environmental (MOSTI) under Science Fund grant (no. 6013338) and USM Research University grant (no. 814004) for providing the financial support throughout my Master study.

Most importantly, I would like to thank my father Lam Fook Cheon, my mother Kan Lai Leng, my sister Lam Sze Hui and my brother Lam Wei Hong for their unconditional love and continued support and care. I dedicate this work to them

TABLE OF CONTENTS

	Page
ACKNOWLEDGEMENTS	ii
TABLE OF CONTENTS	iii
LIST OF TABLES	vii
LIST OF FIGURES	ix
LIST OF PLATES	xii
LIST OF SYMBOLS	xiii
LIST OF ABBREVIATIONS	xiv
ABSTRAK	xvi
ABSTRACT	xviii
CHAPTER 1 : INTRODUCTION	
1.1 Industrial water pollution	1
1.2 Heterogeneous photocatalysis	2
1.3 Problem statement	4
1.4 Research objectives	7
1.5 Scope of study	7
1.6 Organization of the thesis	8
CHAPTER 2 : LITERATURE REVIEW	
2.1 Properties of phenol	11
2.1.1 Properties and application of phenol	11
2.1.2 Phenol in environment and its toxicity	13
2.2 Advance oxidation processes	14
2.3 Heterogeneous photocatalysis	16
2.3.1 Mechanism of heterogeneous photocatalysis	18
2.4 Semiconductor photocatalysts	22
2.4.1 Nanosized TiO ₂ photocatalyst	26
2.5 Synthesis of immobilized TiO ₂ films	28

2.5.1	Sol-gel method	28
2.5.2	Sol-gel synthesis of immobilized TiO ₂ -P25 films	31
2.6	Photocatalyst supports	34
2.6.1	Activated carbon	36
2.7	Photocatalytic reactors	39
2.8	Effect of process variables	42
2.8.1	UV light intensity	43
2.8.2	Solution pH	44
2.8.3	Presence of electron acceptor	45
2.8.4	Photocatalyst loading	46
2.8.5	Initial concentration of substrate	48
2.9	Design of experiment	48
2.9.1	Response surface methodology	49

CHAPTER 3 : EXPERIMENTAL

3.1	Materials and chemicals	55
3.2	Equipments	56
3.2.1	Fluidized bed reactor	56
3.2.2	High performance liquid chromatograph (HPLC)	61
3.2.3	Total organic carbon (TOC) spectrophotometer	61
3.2.3	Viscosity measurement	62
3.3	Preparation of photocatalyst	62
3.3.1	Preparation of modified sol-gel	62
3.3.2	Immobilization of TiO ₂ -P25 onto activated carbon (AC)	63
3.4	Characterization of photocatalyst	65
3.4.1	X-ray diffraction (XRD)	65
3.4.2	Scanning electron microscopy (SEM)	65
3.4.3	Energy dispersive X-ray (EDX)	66
3.4.4	Transmission electron microscope (TEM)	66
3.4.5	Surface characteristics	66
3.5	Activity test	67
3.5.1	Preliminary studies	68

3.5.2	Comparison of suspended TiO ₂ and TPA photocatalysts	69
3.5.2.1	Repeatability of photocatalysts	69
3.5.2.2	Mineralization studies of phenol	69
3.5.3	Desorption of phenol which absorbed on AC	69
3.6	Process variable studies	70
3.6.1	Effect of UV light intensity	70
3.6.2	Effect of solution pH	70
3.6.3	Effect of air flow rate	71
3.6.4	Effect of photocatalyst loading	71
3.6.5	Effect of initial phenol concentration	71
3.7	Statistical design of experiment	72

CHAPTER 4 : RESULTS AND DISCUSSION

4.1	Preliminary studies	76
4.2	Effect of calcination temperature on photocatalyst preparation	80
4.2.1	Photocatalyst characterization	80
4.2.1.1	X- ray diffraction (XRD)	80
4.2.1.2	Transmission electron microscopy (TEM)	83
4.2.1.3	Surface characteristics	86
4.2.2	Photocatalytic performance	88
4.3	Effect of P25 loading on photocatalyst preparation	92
4.3.1	Photocatalyst characterization	92
4.3.1.1	X- ray diffraction (XRD)	92
4.3.1.2	Scanning electron microscopy (SEM)	95
4.3.1.3	Energy dispersive X-ray (EDX)	100
4.3.1.4	Transmission electron microscopy (TEM)	104
4.3.1.5	Surface characteristics	107
4.3.1.6	Viscosity and film weight	110
4.3.2	Photocatalytic performance	112
4.4	Comparison of suspended TiO ₂ and TPA photocatalysts	117
4.4.1	Repeatability of photocatalyst	117
4.4.2	Mineralization studies of phenol	120

4.5	Desorption of phenol which adsorbed on AC	123
4.6	Process variable studies	126
4.6.1	Effect of UV light intensity	127
4.6.2	Effect of solution pH	129
4.6.3	Effect of air flow rate	133
4.6.4	Effect of photocatalyst loading	136
4.6.5	Effect of initial substrate concentration	139
4.7	Kinetic studies	143
4.7.1	Photocatalytic degradation kinetics of phenol	143
4.7.2	Reaction order and apparent rate constant	145
4.7.3	Langmuir-Hinshelwood model	147
4.7.4	Initial reaction rate	149
4.8	Optimization studies using response surface methodology	152
4.8.1	Model fitting	152
4.8.2	Analyses of variance (ANOVA)	154
4.8.3	Response surface plot	157
4.8.3.1	Effect of photocatalyst loading and solution pH	158
4.8.3.2	Effect of photocatalyst loading initial phenol	159
4.8.3.3	Effect of initial phenol and solution pH	160
4.8.4	Optimum condition and verification	161

CHAPTER 5 : CONCLUSIONS AND RECOMMENDATIONS

5.1	Conclusions	164
5.2	Recommendations	167

REFERENCES	169
-------------------	-----

APPENDIX		
Appendix A	Calibration curve	196

LIST OF PUBLICATIONS	197
-----------------------------	-----

LIST OF TABLES

	Page	
Table 2.1	Chemical and physical properties of phenol (Busca <i>et al.</i> , 2008)	12
Table 2.2	The oxidizing potential of different oxidants (Molinari <i>et al.</i> , 2004)	15
Table 2.3	Example of AOPs used to produce the reactive hydroxyl radical	16
Table 2.4	Organic pollutants mineralized by heterogeneous photocatalysis	17
Table 2.5	Band gap energy (E_{bg}) and wavelength (λ) of semiconductors (Bhatkhande <i>et al.</i> , 2001)	23
Table 2.6	Presentation of different methods used to prepare supported TiO ₂ film (Guillard <i>et al.</i> , 2002)	30
Table 2.7	Classification of activated carbon pore sizes (Corrott <i>et al.</i> , 1999)	37
Table 2.8	Heterogeneous photocatalytic reactors (Cassano and Alfano, 2000)	40
Table 2.9	Effect of photocatalyst loading on the photocatalytic degradation of pollutants	47
Table 3.1	List of chemicals and reagents	56
Table 3.2	Fluidized bed reactor and UV light specifications	58
Table 3.3	Process variables and their range in phenol degradation study	72
Table 3.4	The range and levels of each variable in CCD	73
Table 3.5	The 2 ³ factorial and CCD experiment matrix	74
Table 4.1	Characteristics of the TPA1 photocatalyst prepared at different calcination temperatures	82
Table 4.2	BET surface area (S_{BET}), total pore volume (V_{tot}) and average pore size (D) of TPA1 photocatalyst prepared at different calcination temperatures	87

Table 4.3	Characteristics of the TA-600 and TPA-600 photocatalyst prepared at different P25 loadings	94
Table 4.4	Elemental composition of TA-600, TPA3-600 and original AC	102
Table 4.5	BET surface area (S_{BET}), total pore volume (V_{tot}) and average pore width (D) of synthesized photocatalysts	107
Table 4.6	Variation of film weight with change in viscosity of sol	111
Table 4.7	TOC removals of suspended TiO_2 and TPA3-600 for phenol degradation	121
Table 4.8	The values of the apparent rate constant (k_{app}) and correlation coefficient (R^2) at different phenol concentrations	147
Table 4.9	The values of k_{L-H} and K obtained in the phenol degradation	151
Table 4.10	Experimental design matrix and response based on phenol degradation	153
Table 4.11	Sequential model sum of squares	154
Table 4.12	ANOVA for the quadratic model of phenol degradation	155
Table 4.13	Independent variables, response and their desired goal for optimizing phenol degradation	162
Table 4.14	Reproducibility test for response at optimum condition	163

LIST OF FIGURES

		Page
Figure 2.1	Illustration of different processes on a photocatalyst upon excitation (Beydoun <i>et al.</i> , 1999)	19
Figure 2.2	Photocatalytic degradation of phenol by nanosized TiO ₂ (Guo <i>et al.</i> , 2004)	22
Figure 2.3	Energy level diagram for semiconductors in aqueous media at pH = 0 (Gaya and Abdullah, 2008)	24
Figure 2.4	Crystal structure of (a) anatase and (b) rutile (Carp <i>et al.</i> , 2004)	25
Figure 2.5	Macropore, mesopore and micropore adsorption sites on activated carbon (Tchobanoglous <i>et al.</i> , 2003)	37
Figure 2.6	Comparison of the three types of CCD for two factors	52
Figure 3.1	Schematic diagram of fluidized bed reactor	60
Figure 3.2	Flow chart of the TPA photocatalyst preparation	64
Figure 3.3	Schematic diagram of CCD as a function of X_1 , X_2 , and X_3 (Cho and Zoh, 2007)	74
Figure 4.1	Comparison of in the dark, photolysis, adsorption and photocatalytic degradation rate of phenol. (UV light intensity = $921 \mu\text{W}/\text{cm}^2$; air flow rate = 2 L/min; [TiO ₂ -P25] = 0.41 g/L; [phenol] = 50 mg/L)	78
Figure 4.2	XRD pattern of TPA1 prepared at different calcination temperature (A: anatase; R: rutile)	81
Figure 4.3	TEM images of TPA1 prepared at (a) 400°C, (b) 500°C, (c) 600°C and (d) 700°C	84
Figure 4.4	Effect of calcination temperature on the degradation rate of phenol. (UV light intensity = $921 \mu\text{W}/\text{cm}^2$; air flow rate = 2 L/min; [TiO ₂ -P25] = 0.36 g/L; [phenol] = 50 mg/L)	89
Figure 4.5	XRD patterns of the TPA-600 prepared at different P25 loadings (A: anatase; R: rutile)	93
Figure 4.6	SEM images of (a) TA-600, (b) TPA1-600, (c) TPA3-600 and (d) TPA6-600	96

Figure 4.7	SEM images of (a) TPA3-600 and (b) TPA6-600	97
Figure 4.8	EDX spectra of TA-600 photocatalyst	100
Figure 4.9	EDX spectra of TPA3-600 photocatalyst	101
Figure 4.10	EDX spectra of original AC	101
Figure 4.11	TEM images of (a) TA-600 and TPA-600 prepared at (b) 1 g/L P25 powder, (c) 3 g/L P25 powder and (d) 6 g/L P25 powder	105
Figure 4.12	Effect of P25 loading on the degradation rate of phenol. (UV light intensity = $921 \mu\text{W}/\text{cm}^2$; air flow rate = 2 L/min; $[\text{TiO}_2\text{-P25}] = 0.41 \text{ g/L}$; $[\text{phenol}] = 50 \text{ mg/L}$)	113
Figure 4.13	Degradation rate of suspended TiO_2 and TPA3-600 for phenol degradation of five cycles. (UV light intensity = $921 \mu\text{W}/\text{cm}^2$; air flow rate = 2 L/min; $[\text{TiO}_2\text{-P25}] = 0.41 \text{ g/L}$; $[\text{phenol}] = 50 \text{ mg/L}$)	118
Figure 4.14	Reaction paths of mineralization of phenol over (a) TPA3-600 and (b) suspended TiO_2 (Zhang <i>et al.</i> , 2005)	122
Figure 4.15	Concentration of phenol extracted from TPA3-600 after being treated to phenol in the adsorption and photocatalysis processes. (UV light intensity = $921 \mu\text{W}/\text{cm}^2$; air flow rate = 2 L/min; $[\text{TiO}_2\text{-P25}] = 0.41 \text{ g/L}$; $[\text{phenol}] = 50 \text{ mg/L}$)	124
Figure 4.16	Effect of UV light intensity on the degradation rate of phenol. (UV $\lambda = 254 \text{ nm}$; solution pH = 5.2 air flow rate = 2 L/min; $[\text{TiO}_2\text{-P25}] = 0.41 \text{ g/L}$; $[\text{phenol}] = 50 \text{ mg/L}$)	127
Figure 4.17	Effect of solution pH on the degradation rate of phenol. (UV light intensity = $921 \mu\text{W}/\text{cm}^2$; air flow rate = 2 L/min; $[\text{TiO}_2\text{-P25}] = 0.41 \text{ g/L}$; $[\text{phenol}] = 50 \text{ mg/L}$)	130
Figure 4.18	Effect of air flow rate on the degradation rate of phenol. (UV light intensity = $921 \mu\text{W}/\text{cm}^2$; solution pH = 5.2; $[\text{TiO}_2\text{-P25}] = 0.41 \text{ g/L}$; $[\text{phenol}] = 50 \text{ mg/L}$)	134
Figure 4.19	Effect of photocatalyst loading on the degradation rate of phenol. (UV light intensity = $921 \mu\text{W}/\text{cm}^2$; solution pH = 5.2; air flow rate = 2 L/min; $[\text{phenol}] = 50 \text{ mg/L}$)	137
Figure 4.20	Effect of initial phenol concentration on the degradation rate of phenol. (UV light intensity = $921 \mu\text{W}/\text{cm}^2$; solution pH = 5.2; air flow rate = 2 L/min; $[\text{TiO}_2\text{-P25}] = 0.41 \text{ g/L}$)	140

Figure 4.21	Kinetics of phenol degradation for different phenol concentrations in the presence of TPA3-600. (UV light intensity = $921 \mu \text{W}/\text{cm}^2$; solution pH = 5.2; air flow rate = 2 L/min; $[\text{TiO}_2\text{-P25}] = 0.41 \text{ g/L}$)	146
Figure 4.22	$1/r$ as a function $1/C$ plot for phenol degradation	150
Figure 4.23	Parity plot of experimental and predicted values of phenol degradation	157
Figure 4.24	Response surface plot for degradation rate of phenol as function of solution pH and photocatalyst loading (initial phenol concentration = 25 mg/L)	159
Figure 4.25	Response surface plot for degradation rate of phenol as function of initial phenol concentration and photocatalyst loading (solution pH = 5)	160
Figure 4.26	Response surface plot for degradation rate of phenol as function initial phenol concentration and solution pH (photocatalyst loading = 2 layers)	161
Figure A-1	Calibration curve of phenol obtained from HPLC analysis	198

LIST OF PLATES

	Page
Plate 3.1 Fluidized bed reactor	59
Plate 3.2 UV light enclosure with the quartz column	59
Plate 3.3 Main reaction chamber (quartz column)	60

LIST OF SYMBOLS

Symbol	Description	Unit
C	Phenol concentration at time t	mg/L
C_o	Initial phenol concentration	mg/L
cb	Conduction band	-
cp	Centipoise	Kg/m.s
dc/dt	Differential of C polynomial with respect to t	-
e^-	Electron	-
h^+	Hole	-
$HO_2\bullet$	Hyperoxyl radical	-
K	Adsorption equilibrium rate constant	L/mg
k_{app}	Pseudo-first-order rate constant	1/min
k_{L-H}	Reaction rate constant	mg/L.min
$O_2\bullet^-$	Superoxide radical anion	-
OH^-	Hydroxyl ion	-
$\bullet OH$	Hydroxyl radical	-
pH_{pzc}	Point of zero charge	-
R^2	coefficient of correlation	-
r	Reaction rate	mg/L.min
t	Time	min
T	Temperature	°C
wt. %	Weight in percent	g

Greek symbols

λ	Wavelength	nm
α	Alpha (axial distance from the center point which makes the design rotatable)	-
θ	Surface coverage	-

LIST OF ABBREVIATIONS

AC	Activated carbon
ANOVA	Analysis of variance
AOPs	Advance oxidation processes
ATSDR	Agency for Toxic Substances and Disease Registry
BET	Brunauer-Emmett-Teller
CCD	Central composite design
CO ₂	Carbon dioxide
CV	Coefficient of variation
3D	Three dimensional
DEA	Diethanolamine
<i>DF</i>	Degree of freedom
DI	Deionized water
DOE	Department of Environment
E_{bg}	Band gap energy
EDX	Energy dispersive X-ray
EHC	Environmental Health Criteria
<i>F</i> -value	Fisher value
FBR	Fluidized bed reactor
HCl	Hydrochloric acid
HNO ₃	Nitric acid
H ₂ O	Water
H ₂ O ₂	Hydrogen peroxide
HPLC	High performance liquid chromatograph
<i>i</i> -PrOH	Isopropanol
K	Potassium
L-H	Langmuir-Hinshelwood
O ₂	Oxygen
Ox	Oxidation
<i>Prob</i> > <i>F</i>	Probability value greater than Fisher value
Na	Sodium
NaOH	Sodium hydroxide

NHE	Normal hydrogen electrode
Red	Reduction
RSM	Response surface methodology
SEM	Scanning electron microscopy
Si	Silicone
TiO ₂	Titanium dioxide
TiO ₂ -P25 film	P25 powder added in titanium dioxide film
TEM	Transmission electron microscopy
TOC	Total organic carbon
TTIP	Titanium tetraisopropoxide
USEPA	United State Environment Protection Agency
UV light	Ultra-violet light
vb	Valence band
XRD	X-ray diffraction

DEGRADASI PEMFOTOMANGKINAN FENOL DALAM REAKTOR TERBENDALIR MENGGUNAKAN TiO₂- P25/KARBON TERAKTIF DARIPADA KAEDAH MODIFIKASI SOL-GEL

ABSTRAK

TiO₂-P25 immobilisasi pada karbon teraktif (TPA) telah berjaya disediakan daripada kaedah modifikasi sol-gel. Kajian ini termasuk optimisasi bagi suhu kalsinasi and bebanan P25 dalam penyediaan fotomangkin. Eksperimen untuk degradasi pemfotomangkinan di dalam lapisan terbendalir reaktor menunjukkan bahawa aktiviti pemfotomangkinan bagi fotomangkin yang tersedia boleh ditingkatkan dengan menambah suhu kalsinasi dari 400 ke 600°C, di mana ia disebabkan oleh penambahan kedua-dua kehaburan anatis and rutil dan penambahan sedikit dalam luas permukaan BET, jumlah kandungan lubang dan purata saiz lubang. Ia didapati bahawa optimum suhu kalsinasi dalam penyediaan fotomangkin adalah 600°C. Keputusan telah menunjukkan bahawa penambahan bebanan P25 dibawah lingkungan tertentu (sehingga 3 g/L) boleh meningkatkan aktiviti pemfotomangkinan disebabkan oleh penurunan dalam saiz hablur, penambahan dalam luas permukaan BET, jumlah kandungan lubang dan purata saiz lubang dan penambahan dalam kelikatan sol dan keberatan saput tipis dalam fotomangkin yang tersedia. Analisa EDX juga menyatakan bahawa kehadiran logam asing seperti K, Na dan Si dalam permukaan salut tipis fotomangkin. Nilai optimum bebanan P25 dalam penyediaan fotomangkin adalah didapati 3 g/L. Fotomangkin yang tersedia didapati stabil untuk diulang semula setelah lima kali degradasi fenol and ia juga mempunyai penghapusan TOC yang lebih tinggi daripada butiran TiO₂. Sesetengah fenol yang dijerapkan pada fotomangkin masih dijumpai apabila semua fenol telah dikeluarkan

daripada bendalir. Fenol yang dijerapkan ini boleh didegradasi oleh $\text{TiO}_2\text{-P25}$ yang telah disinari jika UV sinaran dikekalkan berterusan. Kesan daripada pembolehubah-pembolehubah proses seperti intensiti lampu UV, pH bendalir dan kadar aliran udara, bebanan fotomangkin dan kepekatan awal bahan tindak balas telah dikaji. Keadaan-keadaan optimum adalah berikut: intensiti lamp UV $921 \mu \text{W/cm}^2$, pH bendalir 5.2, kadar aliran udara 2 L/min, bebanan fotomangkin 2 lapis dan kepekatan awal fenol 25 mg/L. Kinetik bagi degradasi fenol juga dianalisa. Keputusan menunjukkan bahawa kinetik bagi reaksi ini mematuhi model Langmuir-Hinshelwood dan nilai untuk pemalar kadar (k_{L-H}) dan pemalar jerapan (K) adalah didapati seperti 1.644 mg/L.min dan 1.686×10^{-2} L/mg masing-masing. Di samping itu, metodologi permukaan sambutan (RSM) berdasarkan kepada rekabentuk pusat gabungan (CCD) telah digunakan untuk menilai kesan pembolehubah-pembolehubah kritikal pada degradasi fenol. Model tersebut telah mencadangkan bahawa maksimum kadar degradasi fenol sekurang-kurangnya pada 99.3% akan tercapai dengan keadaan optimum yang ditetapkan pada bebanan fotomangkin 2 lapis, pH bendalir 7 dan kepekatan awal fenol 25 mg/L.

PHOTOCATALYTIC DEGRADATION OF PHENOL IN FLUIDIZED BED REACTOR USING TiO₂-P25/ACTIVATED CARBON PREPARED BY MODIFIED SOL-GEL METHOD

ABSTRACT

TiO₂-P25 immobilized on activated carbon (TPA) was successfully prepared by modified sol-gel method. The study included optimization of calcination temperature and P25 loading in the photocatalyst preparation. Experiments on the photocatalytic degradation of phenol in a fluidized bed reactor showed that the photocatalytic activity of the prepared photocatalyst can be significantly improved by increasing the calcination temperature from 400 to 600°C, which was due to an increase in both the anatase and rutile crystalline material and increase slightly in BET surface area, total pore volume and average pore size. It was found that the optimum calcination temperature in the photocatalyst preparation was 600°C. The results revealed that increasing P25 loading within a certain range (up to 3 g/L) could significantly improve the photocatalytic activity because of a decreased in crystal size, increased in BET surface area, total pore volume and average pore size and increased in viscosity in the sol and film weight of prepared photocatalyst. EDX analysis also showed that the presence of K, Na and Si on the surface of the photocatalyst films. The optimum P25 loading in the photocatalyst preparation was found to be 3 g/L. The prepared photocatalyst was stable for repeated usage after five cycles of phenol degradation and had TOC removal better than the suspended TiO₂. Some phenol remained adsorbed on the photocatalyst when no traces of phenol were detected in the solution. This adsorbed phenol could be degraded by illuminated TiO₂-P25 while maintaining UV irradiation. The effect of process variables such as

UV light intensity, solution pH, air flow rate, photocatalyst loading and initial substrate concentration were examined. The optimum conditions were as follows: UV light intensity of $921 \mu\text{W}/\text{cm}^2$, solution pH 5.2, air flow rate of 2 L/min, photocatalyst loading of 2 layers and initial phenol concentration of 25 mg/L. The kinetic of the phenol degradation was also analyzed. The results indicated that the kinetics of this reaction fitted the Langmuir-Hinshelwood model well and the value of the reaction rate constant (k_{L-H}) and the adsorption equilibrium constant (K) were found as 1.644 mg/L.min and 1.686×10^{-2} L/mg, respectively. In addition, response surface methodology (RSM) based on central composite design (CCD) was applied to access the effect of critical variables on the degradation of phenol. The model predicted maximum degradation rate of phenol of at least 99.3% was achieved with an optimum condition set at photocatalyst loading of 2 layers, solution pH 7 and initial phenol concentration of 25 mg/L.

CHAPTER 1

INTRODUCTION

Pollution refers to contamination of the environment by harmful and waste materials, which brings about a significant change in the quality of the surrounding atmosphere. Environmental pollution can be classified as air pollution, water pollution and noise pollution. Water pollution also signifies contamination of water bodies, which make them unfit for drinking and other uses. Although 70% of the earth is covered by water, the water from the seas and the oceans is saline and thus cannot be used for drinking, agriculture and industrial uses. Only the water bodies like lakes, ponds, rivers, reservoirs and streams provide users with fresh water.

1.1 INDUSTRIAL WATER POLLUTION

Water pollution is caused by emission of domestic or urban sewage, agricultural waste, pollutants and industrial effluents into water bodies. One of the main sources of water pollution is the organic pollutants discharged by industrial units, also known as industrial water pollution (World Resource Institute, 2007). Organic pollutants like phenols and phenolic compounds, dyestuff consisting complicated aromatic rings, petroleum products such as oils and greases, polychlorinated biphenyl (PCB) compounds, pesticides, paints and lubricants are discharged into the water bodies by many industrial units. The organic pollutants discharged into the water bodies usually dissolve or remain suspended in water. Nowadays, fresh water is facing greater stresses and chemical and bacteriological contamination of water bodies has become an issue of increasing concern. As a result, the control of organic pollutants has received much attention for its

considerable amount and variety. Innovative water and wastewater technologies are needed to meet the challenges of deteriorating water quality.

Phenols are one of the most common organic water pollutants since they are harmful to organisms at low concentrations and many of them have been classified as hazardous pollutants because of their potential to harm human health. Chronic toxic effects due to phenols reported in humans include vomiting, difficulty in swallowing, anorexia, liver and kidney damage, headache, fainting and other metal disturbances (Kamble *et al.*, 2007). Accordingly, they are listed by Malaysia's Environmental Quality Regulations 1979 as a priority pollutant with a maximum contamination level in inland waters set at 0.2 mg/L (DOE, 1979). However, phenols are widely used in the industries of petroleum refining, coal tar, steel, dyestuff, synthetic resins, coal gasification and often released in wastewater. Due to their toxicity and recalcitrant nature, phenols are resistant to destruction by biological treatment. Physical methods such as carbon adsorption and air stripping are not destructive but only transfer the pollutants from one phase to another (Carp *et al.*, 2004; Senthikumaar *et al.*, 2006). In addition, conventional chemical methods are not effective when pollutant concentration is low or refractory to the oxidants. Thus, the development of more and effective technologies for phenol remediation becomes important.

1.2 HETEROGENEOUS PHOTOCATALYSIS

Heterogeneous photocatalysis, one of the so called Advanced Oxidation Processes (AOPs) has been utilized to remove a wide range of organic pollutants both in air and water pollution over the past several decades (Linsebigler *et al.*, 1995;

Hoffmann *et al.*, 1995; Fujishima *et al.*, 2000; Gogate and Pandit, 2004; Chiou and Juang, 2007; Chen *et al.*, 2009). The preferential used and already with some practical application are TiO₂ based photocatalysts due to their excellent photocatalytic activity, non-toxic and photochemical stability. In addition, the most attention has been paid to the nanoscale TiO₂ owing to their markedly different physical and chemical properties with respect to bulk materials (Beydoun *et al.*, 1999; Reddy *et al.*, 2001; Liu *et al.*, 2008). This technology is based on the in situ generation of nonselective and highly reactive radicals such as hydroxyl radicals ($\bullet\text{OH}$ radicals) as initiators of the oxidative degradation. Through irradiation of aqueous TiO₂ photocatalyst offers an oxidation capable of pollutant abatement and mineralizes organic pollutants into CO₂, H₂O, NO₃⁻, PO₄³⁻ and halides ions (Carp *et al.*, 2004; Gaya and Abdullah *et al.*, 2008).

So far, heterogeneous photocatalysis has been proven to be able to achieve the following:

- (1) A wide variety of organic pollutants in aqueous and gaseous media can be completely degraded or mineralized,
- (2) Heterogeneous photocatalysis can be used to inactivate pathogenic organisms including bacteria and viruses,
- (3) Dissolved metal ions can be removed in their metallic form through photocatalytic reduction and
- (4) Photocatalytic reactions take place under ambient condition and no other chemicals are required.

The basic photophysical and photochemical principles underlying TiO₂-based heterogeneous photocatalysis are already established and have been reported in many literatures. The degradation of organic pollutants is mediated by a series of reactions initiated by these primary oxidizing species, •OH radicals (Linsebigler *et al.*, 1995; Hoffmann *et al.*, 1995; Fujishima *et al.*, 2000; Bizani *et al.*, 2006; Gaya and Abdullah *et al.*, 2008). The photocatalytic efficiency of the TiO₂-based heterogeneous photocatalysis process depends on several variables such as reactor design, light intensity, organic pollutant, solution pH, oxidizing agent and photocatalyst surface composition (Konstantinou *et al.*, 2004; Sleiman *et al.*, 2007). Moreover, the adsorption of organic pollutants onto the surface of TiO₂ plays an important role in the photocatalytic degradation (Carp *et al.*, 2004; Zhang *et al.*, 2005).

The key feature of TiO₂-based heterogeneous photocatalysis is that TiO₂ produces strong oxidants. However, owing to the cover by the solid-liquid interface and the limitation of organic pollutants available at TiO₂ surface more details on the photocatalytic degradation are difficult to establish and the rate of reactions in the aqueous phase are usually slow. Therefore, even though great advances have been achieved in the understanding of heterogeneous photocatalysis, there are still fundamental and engineering aspects that require clarification.

1.3 PROBLEM STATEMENT

Currently, there are two types of TiO₂ photocatalysts are used in studies concerning water treatment. Those that utilize powder type TiO₂ photocatalysts in suspension and those that utilize film type TiO₂ photocatalysts immobilized on a

support. Although characterized by larger catalytic surface area and absence of mass transfer limitations, systems with suspended TiO₂ impose the requirement for filtering the effluent to remove TiO₂ ultrafine particles of nanoscale dimensions. This filtration process is tedious and costly. Furthermore, it requires several other unit operations and separation processes and does not guarantee complete removal of the ultrafine particles. As a result, current research activities are centered on the area of photocatalysis using immobilized catalyst (Bu *et al.*, 2004; Chen and Dionysiou, 2006a; Ghamsari and Bahramian, 2008).

However, simple immobilization of catalyst over supports often leads to low photocatalytic activity because of its low TiO₂ dispersion and its contact with light as well as introducing a possible mass transfer limitation (Li and Liu, 2003; Balasubramaniam *et al.*, 2004; Chen and Dionysiou, 2006b; Liu *et al.*, 2007). Escape of TiO₂ particles from the supports has also been observed after a period of usage and not suitable for recycling. Recently, several authors have employed commercial TiO₂ powder (Degussa P25) as filler into titanium precursor sol to form composite film to both maintain dispersion and stable film because of their high purity, availability and relatively low cost (Balasubramaniam *et al.*, 2003; Keshmiri *et al.*, 2004; Chen and Dionysiou, 2006a; Chen and Dionysiou, 2007). Moreover, titanium precursor sol could act as a binder (matrix) around Degussa P25 to immobilize P25 particles on the substrates. The advantage of using this technique for the preparation of TiO₂ films is that the high purity Degussa P25 powder can be well immobilized by the presence of sol-gel derived matrix (Chen *et al.*, 2009).

During the recent years, some sorbents that can act as the photocatalyst support have drawn the attention of researchers. These sorbents used often contain silica gel, activated carbon and zeolite (Hisanaga and Tanaka, 2002; Tryba *et al.*, 2007; Meng *et al.*, 2008). The sorbents are so selected that they can be easily suspended by air bubbling or mechanical stirring. Among these sorbents, activated carbon (AC) is an excellent alternative because of its high adsorption capacity and relatively low cost. Furthermore, adding AC to TiO₂ could induce some beneficial effect because of the highly adsorptive characteristic of AC with respect to organic molecules and also resolve the problem of achieving optimum adsorption strength of the adsorbed molecules on the adsorbent to improve TiO₂ photocatalytic activity (Matos *et al.*, 2007). In fact, other authors have also reported a synergistic effect for AC-supported TiO₂ systems of some organic pollutants in the photocatalytic process (Tybra *et al.*, 2003; Lee *et al.*, 2004a; Li *et al.*, 2006; Matos *et al.*, 2007; Li *et al.*, 2007; Liu *et al.*, 2007; Tybra *et al.*, 2007).

While some of the activity of supported TiO₂ photocatalyst is relatively well understood, design and construction of new light sources as well as photochemical reactors of photocatalytic units still require consideration. Fluidized bed is known as a good chemical reactor due to excellent reactants contact, high mass transfer rate and easy to control the system even for large-scale operations (Kim *et al.*, 2004; Qiu and Zheng, 2007). For the application of photocatalytic reactor for the removal of organic pollutants in wastewater, fluidized bed reactor (FBR) was considered as the proper reactor type for photocatalytic reaction. It is believed that fluidized bed can take advantages of better use of light, easy of system control and good contacting

between target compound and photocatalysts over slurry reactors or fixed bed reactors with supported TiO₂ photocatalysts.

1.4 RESEACRH OBJECTIVES

The aim of this research is to develop a photocatalyst with high photoactivity, which is capable of degrading phenol under UV irradiation. The specific objectives of this research are:

1. To develop TiO₂-P25 immobilized on activated carbon (TPA) synthesized using modified sol-gel method for phenol degradation in a fluidized bed reactor.
2. To characterize the chemical and physical properties of TPA using various characterization techniques.
3. To examine the effects of process variables such as UV light intensity, solution pH, air flow rate, photocatalyst loading and initial phenol concentration on the phenol degradation by experimental approach.
4. To determine the reaction kinetics parameters of phenol degradation based on the Langmuir-Hinshelwood kinetic model.
5. To obtain optimum conditions for phenol degradation using response surface methodology (RSM).

1.5 SCOPE OF STUDY

This research is focused in developing a photocatalyst with high photocatalytic activities to degrade phenol in a fluidized bed reactor (FBR). The

development of photocatalyst includes studying the effects of calcination temperature (400 – 700°C) and P25 loading (0 – 6 g/L) in the sol.

Characterization of the prepared photocatalyst was conducted using X-ray diffraction (XRD), scanning electron microscopy (SEM), energy dispersive X-ray (EDX) and transmission electron microscopy (TEM) and surface characteristic and viscosity and film weight test. The performance of the prepared photocatalyst is then evaluated in different process variables. The study was carried out by varying different process variables such as UV light intensity (210 – 921 μ W/cm²), solution pH (2.0 – 12.0), air flow rate (0.5 – 3.0 L/min), photocatalyst loading (1 – 4 layers) and initial substrate concentration (25 – 130 mg/L). Each variable was selected based on reports in literature and through the process of trial and error. Subsequently, these results were employed for kinetic studies based on the Langmuir-Hinshelwood kinetics model.

The response surface methodology (RSM) using Design Expert software version 6.0.6 (Stat-Ease, Inc., USA) was applied to obtain the optimum conditions of the three variables for the degradation of phenol. The selected variables were the photocatalyst loading (1 – 3 layers), solution pH (3.0 – 7.0) and initial phenol concentration (25 – 75 mg/L).

1.6 ORGANIZATION OF THE THESIS

This thesis consists of five chapters. Chapter 1 (Introduction) provides a brief description of industrial water pollution and the technology of TiO₂-based heterogeneous photocatalysis for the removal of the organic pollutants. This chapter

also includes the problem statement that provides some basis and rationale to identify the research directions and objectives. The objectives and scopes of the study are then elucidated. This is followed by the organization of the thesis.

Chapter 2 (Literature review) elaborates some information concerning phenol and simultaneous phenol control technologies. Some background research in the field related to TiO₂-based heterogeneous photocatalysis including the catalyst properties and potential application of heterogeneous photocatalysis as well as their synthesis approach are also highlighted in this chapter. Various photocatalytic reactors used in supported catalyst are also discussed. This serves as the background information about the specific problems that have to be addressed in this research work.

Chapter 3 (Experimental) describes the details of the materials and chemicals used and the research methodology conducted in this research. Detailed of the experimental setup is explained and shown in this chapter. This is followed by the discussion on the detailed experimental procedures including photocatalyst preparation, photocatalyst characterization, process variables studies and experimental design.

Chapter 4 (Results and discussion) presents and discusses all important findings obtained in this study. This chapter is the main part of the thesis and it comprises of six main sections based on the present experimental work. The main topics in this chapter include preliminary studies, screening of photocatalyst preparations, comparison studies between synthesized photocatalyst and commercial

TiO₂ Degussa P25, process variables studies, kinetic studies and optimization studies.

Chapter 5 (Conclusions and recommendations) summarizes the conclusions drawn from this study. Recommendations for future work arising from this research are also presented in this chapter.

CHAPTER 2

LITERATURE REVIEW

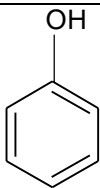
This chapter reviews background information on the subject of heterogeneous photocatalysis process that leads to this research project. It begins with the properties of phenol, advance oxidation processes, heterogeneous photocatalysis, photocatalyst, synthesis of immobilized TiO₂ film, photocatalyst supports, type of photocatalytic reactors and design of experiment.

2.1 PROPERTIES OF PHENOL

2.1.1 Properties and application of phenol

Phenol is a monosubstituted aromatic hydrocarbon. At ambient temperature and pressure, it is a hygroscopic crystalline solid. When pure, solid phenol is white but mostly coloured due to the presence of impurities. This pure compound is mixed with water and commercially sold as a liquid product. Phenol gives off a sweet, acrid smell detectable to most people at about 40 parts of phenol per billion parts (ppb) of air and at about 1 to 8 parts of phenol per million parts (ppm) of water (ATSDR, 2006). It evaporates more slowly than water and is moderately soluble in water. Phenol is also combustible. Table 2.1 summarizes the basic chemical and physical properties of phenol.

Table 2.1. Chemical and physical properties of phenol (Busca *et al.*, 2008).

Structural formula	
Empirical formula	C ₆ H ₅ OH
Molecular weight (g/mol)	94.11
Boiling point (°C)	40.9
Freezing point (°C)	181.75
Water solubility (r.t.)	9.3 g _{phenol} /100 ml _{H2O}
pK _a	9.95
Flammability limits in air (vol %)	Lower limit approximate 1.7 Upper limit 8.6
Flash point (°C)	79 (closed cup)
Auto ignition temperature (°C)	715

Currently, phenol is produced at a rate about 6 million tonnes/year worldwide with a significantly increasing trend (Ray *et al.*, 2009). Processes for the manufacture of phenol include various chemistry and product separation methods. In general, the most widely used process to form phenol is the three-step Hock process (also called the cumene peroxidation method), which produces about 95% of the phenol used in the world. The processes involve the first step, benzene and propylene are reacted to yield cumene, which is purified and oxidized in the second step with oxygen to generate cumene hydroperoxide (CHP). CHP is then isolated and decomposed in the third step with sulfuric acid to obtain phenol along with acetone (Solomons and Fryhle, 2003).

The greater use of phenol is to produce phenolic resins like phenol-formaldehyde resins (Bakelite), which are low-cost thermosetting resins applied as

plywood adhesive, construction, automotive and appliance industries. By reaction with acetone, it may also be converted into bisphenol A, a monomer for epoxy-resins. It is also used to produce cyclohexanone and cyclohexanone-cyclohexanol mixtures by selective catalytic hydrogenation (Weissermel and Arpe, 2003). Cyclohexanone is later converted into its oxime and further to ϵ -caprolactame, the monomer for nylon 6. The mixture cyclohexanone-cyclohexanol is oxidized by nitric acid to adipic acid, one of the monomers for the production of nylon-6, 6. In addition, phenol can be used as a solvent in the production of adhesives, fertilizers, paints, textiles, rubbers, plastic plasticizers and antioxidants (Ray *et al.*, 2009). Other applications include use as a disinfectant for the preparation of some cream and shaving soap for its germicidal and local anesthetic properties and as a reagent in chemical analysis and as a primary petrochemical intermediate.

2.1.2 Phenol in environment and its toxicity

Phenol may enter the atmosphere as fugitive emission from the phenol manufacture and application industries as discussed in above. Release of phenol also occurs during the disposal of industrial wastes. When released into the air, phenol will be degraded by photochemical reactions to dihydroxybenzenes, nitrophenols and ring cleavage products with an estimated half-life in less than 1 day (EHC, 1994). A minor part will disappear from the air by wet deposition (rain).

Phenol is also highly mobile in soil but its transport and reactivity may be affected by pH. It has a relatively short-lived in the soil (generally complete removal in 2 to 5 days). However, phenol can remain in water for a week or more. When released into the water and soil, phenol may be degraded by microbial activity to a

number of organic compounds (Sawyer *et al.*, 1994). The proportion of biodegradation to the overall degradation of phenol is determined by many factors such as concentration, acclimation, temperature and the presence of other compounds.

Exposure to phenol can occur in the workplace or in the environmental following releases to air, water, land or groundwater. Phenol enters body when people breathe air contaminated with phenol or consume food or water contaminated with phenol. It can also be adsorbed through skin contact. Moreover, contact with phenol liquid or vapour can irritate the skin, eyes, nose and throat. Worker breathing large amounts of phenol can experience headaches, muscle weakness, convulsion and coma (ATSDR, 2006). Other human health effects associated with repeated exposure to small amounts of studies show that repeat exposure to phenol in air affects the nervous system of animals. Repeat exposure to large amounts of phenol can also adversely affect the liver, kidneys and the blood of animals (USEPA, 2002). When people are exposed to phenol above the maximum contamination level for relatively short periods of time, anesthetic effects and impaired liver and kidney function may cause. From a lifetime exposure at levels above the phenol, it would result in liver damage, diarrhea, dark urine and red blood cell destruction.

2.2 ADVANCE OXIDATION PROCESSES

Advanced oxidation processes (AOPs) are efficient novel methods useful to accelerate the non-selective and thus the destruction of wide range of organic pollutants resistant to conventional technologies (Gogate *et al.*, 2002). AOPs are based on physicochemical process that produce in situ powerful oxidizing species,

mainly hydroxyl radicals ($\bullet\text{OH}$) by using chemical and/or other forms of energy. Table 2.2 lists the relative oxidizing power of the $\bullet\text{OH}$ radical along with other common oxidants.

Table 2.2. The oxidizing potential of different oxidants (Molinari *et al.*, 2004).

Oxidation species	Oxidation potential, <i>eV</i>
Fluorine	3.06
Hydroxyl radical	2.80
Nascent oxygen	2.42
Ozone	2.07
Hydrogen peroxide	1.77
Perhydroxyl radical	1.70
Hypochlorous Acid	1.49
Chlorine	1.36

As shown, with the exception of fluorine, the $\bullet\text{OH}$ radical is one of the most active oxidants known. The $\bullet\text{OH}$ radical reacts with the dissolved pollutants and initiating a series of oxidation reactions until the pollutants are converted completely to carbon dioxide, water and innocuous mineral salts (Konstantinou and Albanis, 2004; Pekakis *et al.*, 2006; Gaya and Abdullah, 2008). Non-selective in their mode of attack and able to operate at normal temperature and pressure, $\bullet\text{OH}$ radicals are capable of oxidizing almost all reduced materials present without restriction to specific classes of groups of pollutants as compared to other oxidants.

At the present time, a variety of AOPs are available to produce $\bullet\text{OH}$ in the gaseous and aqueous phases. Some of the AOPs reported in the literatures are shown in Table 2.3. Of the AOPs reported in Table 2.3, only ozone/UV, ozone/H₂O₂,

ozone/UV/H₂O₂ and H₂O₂/UV are being used on a commercial scale (Tchobanoglous *et al.*, 2003).

Table 2.3. Example of AOPs used to produce the reactive hydroxyl radical.

Advance oxidation processes	References
Ozone + UV	Benitez <i>et al.</i> (2002) and Hsing <i>et al.</i> (2006)
Ozone + H ₂ O ₂	Sunder and Hempel (1997)
Ozone + UV + H ₂ O ₂	Amiri (2001)
Ozone + TiO ₂	Wang <i>et al.</i> (2002), Beltran <i>et al.</i> (2003) and Sano <i>et al.</i> (2007)
Ozone + ultrasound	Kang and Hoffmann (1998)
H ₂ O ₂ + UV	Korbahti and Rauf (2008)
H ₂ O ₂ + UV + ferrous salts (Fenton's reagent)	Kang <i>et al.</i> (2002), Sun <i>et al.</i> (2007), Secula <i>et al.</i> (2008) and Alaton <i>et al.</i> (2009)
Ultrasonics	Rokhina <i>et al.</i> (2009)
Photocatalysis (UV + TiO ₂)	Hoffmann <i>et al.</i> (1995), Pirkanniemi and Sillanpaa (2002), Carpio <i>et al.</i> (2005), Cho and Zoh (2007), Chiou and Juang (2008) and Naeem and Feng (2009)
Catalysis oxidation	Berndt and Landri (2001), Everaert and Baeyens (2004) and Pelusa <i>et al.</i> (2008)

2.3 HETEROGENEOUS PHOTOCATALYSIS

Among advance oxidation processes (AOPs), heterogeneous photocatalysis on metal oxide semiconductor has been shown to be an effective means of removing a wide range of organic pollutants both in air and water pollution (Herrmann *et al.*, 1999; Fujishima *et al.*, 2000; Chen *et al.*, 2004; Kwon *et al.*, 2006). Compared with conventional wastewater treatments, heterogeneous photocatalysis has the following advantages (Merabet *et al.*, 2009):

- (1) Heterogeneous photocatalysis takes place under ambient condition,
- (2) The degradation and mineralization of a wide variety of organic pollutants in both aqueous and gaseous systems has been demonstrated and
- (3) It can provide a potentially inexpensive and convenient way of treating organic pollutants.

Heterogeneous photocatalysis refers to the photocatalytic reactions in which the pollutants and the photocatalyst comprise two or more phases. In gas system, it usually takes place in gas-solid interface. In aqueous solution, it occurs at solid-liquid interface. The overall process can be decomposed into five independent steps: (1) transfer of pollutants to the surface of the catalyst, (2) adsorption of the pollutant on the surface, (3) reaction on the adsorbed phase, (4) desorption of the product and (5) removal of the product from the interfacial region (Herrmann, 1999).

The photocatalytic reaction occurs in the step (3) upon absorption of a photon, the reactive $\bullet\text{OH}$ radicals are generated on the surface of photocatalyst, which in turn can degrade organic pollutants and totally mineralize them. Table 2.4 exhibits the list of organic pollutants that can be mineralized by heterogeneous photocatalysis.

Table 2.4. Organic pollutants mineralized by heterogeneous photocatalysis.

Class of organics	Examples	References
Haloalkanes/haloalkenes	Chloroform, Trichloroethylene, Acetylene	Wang <i>et al.</i> (1997), Keshmiri <i>et al.</i> (2004) and Thevenet <i>et al.</i> (2005)
Aliphatic alcohols	2-propanol, Methanol	Marci <i>et al.</i> (1995) and Renzi <i>et al.</i> (1997)
Aliphatic carboxylic acids	Formic	Gogate and Pandit (2002)

Table 2.4. Continued

Aromatics	Benzene, Toulene	Hisanaga and Tanaka (2002) and Liu <i>et al.</i> (2006)
Haloaromatics	Chlorobenzene, Monochlorobenzene	Bhatkhande <i>et al.</i> (2004) and Huang <i>et al.</i> (2006)
Phenolic compounds	Phenol	Liu <i>et al.</i> (2007) and Chiou and Juang (2008)
Halophenols	4-nitrophenol, 2,6-dinitrophenol, 4-flurophenol	Chen and Ray (1998), Swarnalatha and Anjaneyulu (2004) and Selvam <i>et al.</i> (2007)
Aromatic carboxylic acids	Benzoic acid, 4-hydroxylbenzoic acid, Salicylic acid	Mehrotra <i>et al.</i> (2005), Lin <i>et al.</i> (2009) and Rao <i>et al.</i> (2009)
Surfactants	Sodium dodecyl sulfate, Nonylphenol polythoxylate, sodium lauryl sulfate	Lea <i>et al.</i> (1998), Horikoshi <i>et al.</i> (2002) and Nam <i>et al.</i> (2009)
Herbicides	Atrazine	Jain <i>et al.</i> (2009)
Pesticides	Oxamyl, Pyridaben, Propoxur	Malato <i>et al.</i> (2000), Zhu <i>et al.</i> (2005) and Mahalakshimi <i>et al.</i> (2009)
Dyes	Methylene Blue, Methyl orange, Orange G, Metanil Yellow, Acid Red 4, Rhodamine B	Chin <i>et al.</i> (2004), Li <i>et al.</i> (2006), Sun <i>et al.</i> (2006), Sleiman <i>et al.</i> (2007), Wang <i>et al.</i> (2008) and He <i>et al.</i> (2009)

2.3.1 Mechanisms of heterogeneous photocatalysis

Heterogeneous photocatalysis as an increase in the rate of a thermodynamically allowed ($\Delta G < 0$) reaction in the presence of photocatalyst with the increase originating from the creation of some new reaction pathways involving photogenerated species and a decrease of the activation energy (Carp *et al.*, 2004). The mechanism of photocatalytic degradation on the surface of photocatalyst is widely accepted as follows (Hoffmann *et al.*, 1995):

- (1) Charge-carrier generation
- (2) Charge-carrier trapping

- (3) Charge-carrier recombination
- (4) Photocatalytic degradation

Charge-carrier generation

As can be seen in Figure 2.1, heterogeneous photocatalysis involves irradiation of photocatalyst such as titanium dioxide (TiO₂) with light energy greater than or equal to the band gap of the photocatalyst and promoting an electron from the valance band to the conduction band (Konstantinou and Albanis, 2004). Then, $e^- - h^+$ pairs are generated as shown in Equation (2.1).

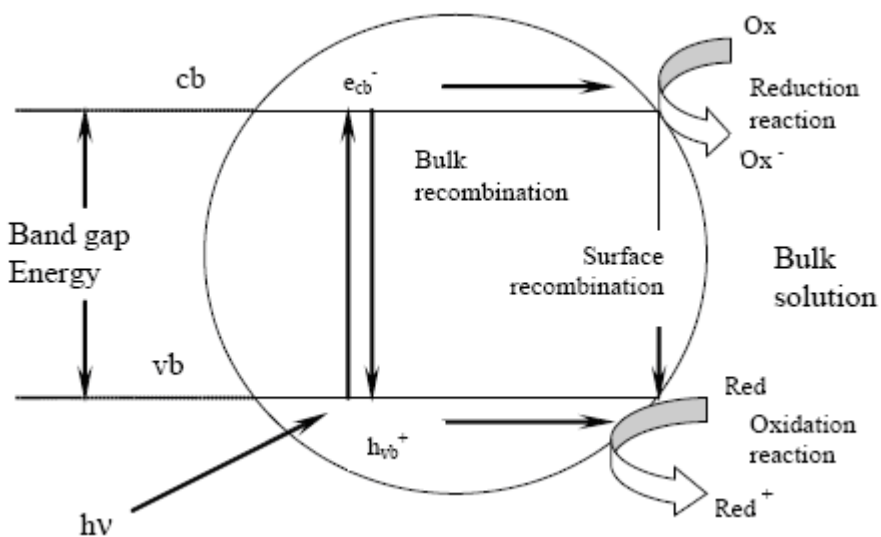
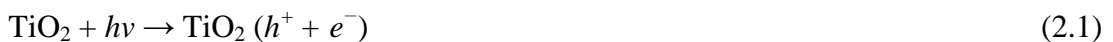


Figure 2.1. Illustration of different processes on a photocatalyst upon excitation (Beydoun *et al.*, 1999).



Charge-carrier trapping

The $e^- - h^+$ pairs is trapped by electron and hole scavengers and inhibited from recombination. The trapped hole is a strong oxidant, which can either oxidize a

pollutant directly or react with electron donor like water and hydroxyl ions (OH⁻) to form •OH radicals (So *et al.*, 2002). The reaction of trapped hole can be expressed in Equations (2.2) and (2.3).



On the other hand, it is important for the trapped electron in the conduction band to be scavenged by an electron acceptor to inhibit its recombination with the trapped hole. One efficient electron acceptor is molecular oxygen (O₂). Through the reduction of O₂ with electron, reactive superoxide radical anions (O₂•⁻) was produced. In addition, other oxidizing species such as hydroxyl radicals (HO₂•) and hydrogen peroxide (H₂O₂) were also formed (Chen *et al.*, 2005; Rauf *et al.*, 2009). It is believed that additional •OH radicals would generate according to the following Equations from (2.4) to (2.10).



Charge-carrier recombination

In competition with charge transfer to adsorbed species, there is the possibility that both $e^- - h^+$ pair recombination and trapped carrier recombination take place. The recombination can occur at the surface and/or volume of the photocatalyst with release of heat as shown in Equation (2.11) (Schiavello, 1997). According to Hoffmann *et al.* (1995), the recombination of $e^- - h^+$ pairs is main factor in limiting oxidation rates of organic pollutants.



Photocatalytic degradation

The Equations (2.1) to (2.11) indicated the important role of $e^- - h^+$ pairs in photocatalytic degradation. Basically, the holes, $\bullet\text{OH}$ radicals, $\text{O}_2\bullet^-$ and $\text{HO}_2\bullet$ are highly reactive intermediates that will participate in photocatalytic degradation of large variety of organic pollutants. The photocatalytic degradation of phenol is interesting mechanistic example on the role of holes, $\bullet\text{OH}$ radicals, $\text{O}_2\bullet^-$ in TiO_2 -assisted heterogeneous photocatalysis of aromatic organic pollutants. The mechanism of the photocatalytic degradation of phenol by nanosized TiO_2 is illustrated in Figure 2.2.

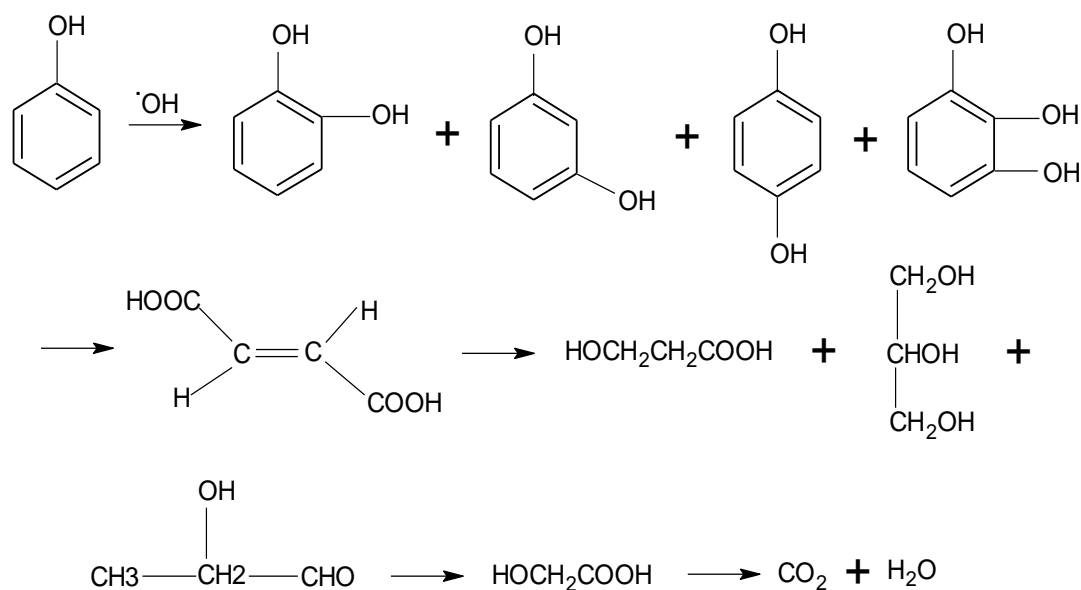


Figure 2.2. Photocatalytic degradation of phenol by nanosized TiO₂ (Guo *et al.*, 2006).

The degradation of phenol leads to several intermediates that have been reported by Sobczynski *et al.* (2004) and Guo *et al.* (2006). The •OH radical attacks the phenyl ring of the phenol yielding catechol, resorcinol, hydroquinone, benzene-1, 2, 3-triol and then the phenyl rings in these compounds break up to give malonic acid together with short-chain organic acids such as maleic, oxalic, acetic, formic and finally CO₂ and H₂O.

2.4 SEMICONDUCTOR PHOTOCATALYSTS

Numerous semiconductors have been used for the photocatalytic degradation of organic pollutants. Most of these semiconductor particles are metal oxides such as TiO₂, WO₃, ZnO, and Fe₂O₃ and metal sulfides such as CdS and PdS (Gaya and Abdullah, 2008). Table 2.5 lists the most common semiconductors employed heterogeneous photocatalysis together with their respective band gap energies and wavelengths.

Table 2.5. Band gap energy (E_{bg}) and wavelength (λ) of semiconductors (Bhatkhande *et al.*, 2001).

Semiconductor	E_{bg} (eV)	λ (nm)
TiO ₂ (anatase)	3.2	388
TiO ₂ (rutile)	3.0	413
ZnO	3.2	388
ZnS	3.6	344
WO ₃	2.8	443
CdS	2.5	496
Fe ₂ O ₃	2.3	539
MoS ₂	1.75	709

In order to explain the potential energy of the photogenerated $e^- - h^+$ pairs and consequently their strength to produce oxidative or reductive pathways, an energy-level diagram is normally used. Figure 2.3 exhibits the energy levels for some of these semiconductors employed in heterogeneous photocatalysis with respect to the normal hydrogen electrode (NHE) at pH = 0. The energy level at the bottom of conduction band is actually the reduction potential of photogenerated electrons. The energy level at the top of valence band determines the oxidizing ability of photogenerated holes and each value reflecting the ability of the system to promote reduction and oxidation reactions (Carp *et al.*, 2004). All semiconductors could be photocatalysts but only some semiconductors show photocatalytic properties.

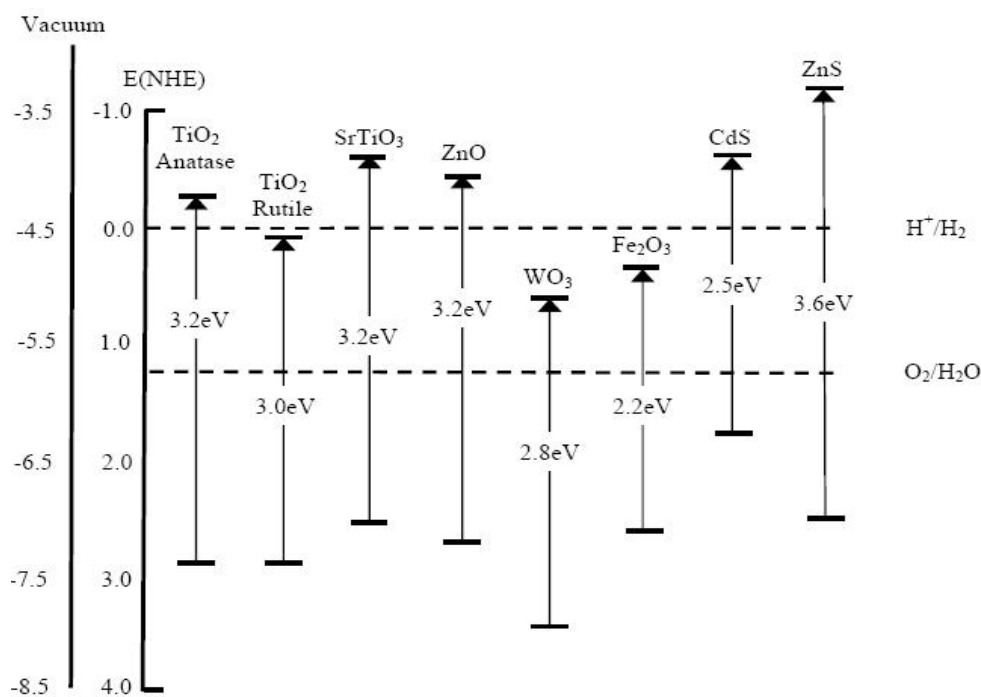


Figure 2.3. Energy level diagram for semiconductors in aqueous media at pH = 0 (Gaya and Abdullah, 2008).

Among the semiconductors reported in Table 2.5, TiO₂ has generally exhibited the highest photocatalytic activity in a wider range of environmental applications. Particularly, TiO₂-assisted heterogeneous photocatalysis offers the following advantages:

- (1) TiO₂ is inexpensive, non-toxic, chemically and biologically inert nature (Keshmiri *et al.*, 2004).
- (2) The light required to activate the photocatalyst is near ultraviolet radiation making the use of solar light possible (Konstantinou and Albanis, 2004; Merabet *et al.*, 2009).
- (3) TiO₂ surface is fully hydroxylated in water with these hydroxyl groups being the precursors of the •OH radicals (Diebold, 2003).

TiO₂ has three different crystalline structures: anatase, rutile and brookite. The rutile phase is the thermodynamically stable form and the anatase phase transfer to rutile phase when the temperature above 700°C (Valtierra *et al.*, 2006). Among these crystal structures, anatase and rutile phases are most studied phases in heterogeneous photocatalysis. The lattice structures of anatase and rutile phases can be described in terms of (TiO₂⁶⁻) octahedrals as illustrated in Figure 2.4. The two crystal structures differ by the distortion of each octahedral and by the assembly patterns of the octahedral chains. Anatase can be regarded to be built up from octahedrals that are connected by their vertices and in rutile, the edges are connected (Carp *et al.*, 2004).

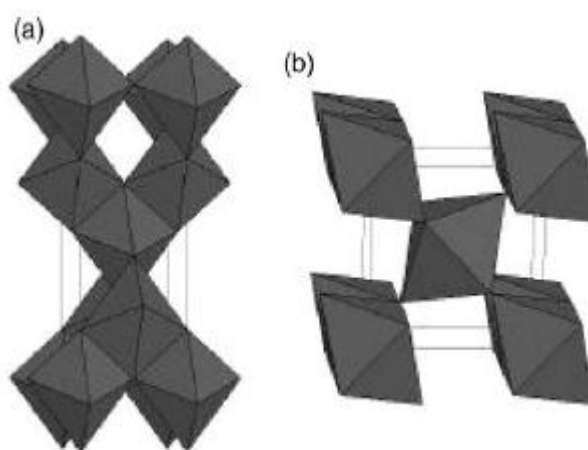


Figure 2.4. Crystal structure of (a) anatase and (b) rutile (Carp *et al.*, 2004).

The difference in lattice structure of anatase and rutile cause different density and electronic band structure leading to different band gap. The minimum band gap energy required for photon to cause photogeneration of charge carriers over anatase and rutile is 3.20 and 3.02 eV, which is corresponding to wavelength of 388 and 413 nm, respectively.